ISSN 1674-1056
http://cpb.iphy.ac.cn
http://iopscience.iop.org/cpb
中国物理 B
Chinese Physics
中国物理 Chinese Physics B

Dynamic evolution of vortex structures induced bytri-electrode plasma actuator

Bo-Rui Zheng(郑博睿)[1], Ming Xue(薛明)[2], Chang Ge(葛畅)[1]
Citation: Chin. Phys. B . 2020, 29(2): 024704 . **doi:** 10.1088/1674-1056/ab671f
Journal homepage: http://cpb.iphy.ac.cn; http://iopscience.iop.org/cpb

What follows is a list of articles you may be interested in

Effect of edge transport barrier on required toroidal field for ignition of elongated tokamak

Cui-Kun Yang(杨翠坤), Ming-Sheng Chu(朱名盛), Wen-Feng Guo(郭文峰)
Chin. Phys. B . 2019, 28(4): 045202 . **doi:** 10.1088/1674-1056/28/4/045202

Electric and plasma characteristics of RF discharge plasma actuation under varying pressures

Huimin Song(宋慧敏), Min Jia(贾敏), Di Jin(金迪), Wei Cui(崔巍), Yun Wu(吴云)
Chin. Phys. B . 2016, 25(3): 035204 . **doi:** 10.1088/1674-1056/25/3/035204

A novel method of evaluating the lift force on the bluff body based on Noca's flux equation

Sui Xiang-Kun, Jiang Nan
Chin. Phys. B . 2015, 24(8): 084701 . **doi:** 10.1088/1674-1056/24/8/084701

Shockwave-boundary layer interaction control by plasma aerodynamic actuation：An experimental investigation

Sun Quan, Cui Wei, Li Ying-Hong, Cheng Bang-Qin, Jin Di, Li Jun
Chin. Phys. B . 2014, 23(7): 075210 . **doi:** 10.1088/1674-1056/23/7/075210

Investigation on the shockwave induced by surface arc plasma in quiescent air

Jin Di, Li Ying-Hong, Jia Min, Li Fan-Yu, Cui Wei, Sun Quan, Zhang Bai-Ling, Li Jun
Chin. Phys. B . 2014, 23(3): 035201 . **doi:** 10.1088/1674-1056/23/3/035201

Dynamic evolution of vortex structures induced by tri-electrode plasma actuator*

Bo-Rui Zheng(郑博睿)[1,†], Ming Xue(薛明)[2], and Chang Ge(葛畅)[1]

[1] School of Automation and Information Engineering, Xi'an University of Technology, Xi'an 710048, China
[2] Department of Aeronautics and Astronautics, Northwestern Polytechnical University, Xi'an 710072, China

(Received 8 November 2019; revised manuscript received 13 December 2019; accepted manuscript online 3 January 2020)

Plasma flow control is a new type of active flow control approach based on plasma pneumatic actuation. Dielectric barrier discharge (DBD) actuators have become a focus of international aerodynamic research. However, the practical applications of typical DBDs are largely restricted due to their limited discharge area and low relative-induced velocity. The further improvement of performance will be beneficial for engineering applications. In this paper, high-speed schlieren and high-speed particle image velocimetry (PIV) are employed to study the flow field induced by three kinds of plasma actuations in a static atmosphere, and the differences in induced flow field structure among typical DBD, extended DBD (EX-DBD), and tri-electrode sliding discharge (TED) are compared. The analyzing of the dynamic evolution of the maximum horizontal velocity over time, the velocity profile at a fixed horizontal position, and the momentum and body force in a control volume reveals that the induced velocity peak value and profile velocity height of EX-DBD are higher than those of the other two types of actuation, suggesting that EX-DBD actuation has the strongest temporal aerodynamic effect among the three types of actuations. The TED actuation not only can enlarge the plasma extension but also has the longest duration in the entire pulsed period and the greatest influence on the height and width of the airflow near the wall surface. Thus, the TED actuation has the ability to continuously influencing a larger three-dimensional space above the surface of the plasma actuator.

Keywords: plasma flow control, dielectric barrier discharge, vortex dynamics, tri-electrode sliding discharge

PACS: 47.32.C–, 52.40.–w, 52.50.Nr **DOI:** 10.1088/1674-1056/ab671f

1. Introduction

Plasma flow control, as a new concept in active flow control technology, is a new research focus in the fields of aerodynamics and aerothermodynamics. Compared with other flow control technologies, plasma flow control is advantageous because it has no moving parts, a short response time and a high bandwidth. A large number of experimental and simulation studies have been performed, and the results show that plasma flow control plays an important role in boundary layer control, flow separation, shear flow, vortex structure and shock wave formation in a flow field, stall separation and aerodynamic noise control, flow resistance reduction, anti- and de-icing, and improvement of combustion stability and efficiency.[1–4]

The pneumatic actuation of a dielectric barrier discharge (DBD) plasma actuator with sinusoidal high-voltage actuation is currently one of the most widely studied plasma flow control methods. A DBD actuator usually consists of two key parts: electrodes and insulating materials. The two electrodes are separated by insulating materials, with one exposed to the air and the other buried in the insulating materials. In most of cases, the positions of the two electrodes are asymmetric with respect to the position of the insulating layer. When a sufficiently high voltage is applied to the electrodes, the air near the surface of the actuator breaks down and is ionized under the strong electric field. For a spatially inhomogeneous electric field, charged ions move due to the electric field gradient. During this directional movement, charged ions collide and exchange momentum with neutral molecules in the air. The air on the surface of the actuator undergoes directional motion, and therefore energy is injected from the plasma zone into the boundary layer to change the aerodynamic characteristics of the air around the objects.

After more than 20-year development, studies on DBD actuators are still in the basic research stage. The typical two-electrode structure of DBD actuator has some shortcomings, such as a small discharge area, low relative induced velocity, and single-direction induced jet, which greatly limit their application in engineering.[5] To solve these problems and improve the energy and efficiency of actuators, researchers have optimized the actuation parameters, such as by changing the electrical parameters and geometric structure of actuation device, but the overall performance improvements are limited.[6–8]

*Project supported by the National Natural Science Foundation of China (Grant No. 51607188), the Foundation for Key Laboratories of National Defense Science and Technology, China (Grant No. 614220202011801), the Shaanxi Provincial Natural Science Basic Research Program, China (Grant No. 2019JM-393), the Shaanxi Provincial Key Industry Innovation, Chain (Grant No. 2017ZDCXL-GY-06-01), and Xi'an Muinicipal Science and Technology Project, China (Grant No. 201805037YD15CG21(28)).

†Corresponding author. E-mail: narcker@xaut.edu.cn

© 2020 Chinese Physical Society and IOP Publishing Ltd

One of the more promising approaches is to add another exposed electrode (sliding electrode) to a typical DBD configuration, thus creating a tri-electrode sliding discharge plasma actuator.[9,10] The aim of using a sliding electrode is to extend the plasma discharge surface over which momentum is exchanged between the plasma zone and the surrounding flow, thereby increasing the surface of plasma actuation for large-scale applications and enhancing the produced body force.

The flow field results show that the structure of the induced flow field will be changed greatly with the polarity and amplitude of the high DC voltage applied to the sliding electrode of the actuator. When the sliding electrode is connected to a high positive DC voltage, it acts as an auxiliary electrode, and only the electric field intensity on the surface of the original DBD actuator is increased, the induced body force will be enhanced; additionally, the fine structure of the induced flow field will be altered due to the influence of the positive DC voltage.[11,12] This discharge morphology is similar to that for DBD actuation and is thus called "extended DBD" (EX-DBD).[13] If the sliding electrode is connected to a high negative DC voltage, it acts as a main electrode, the area of plasma discharge will be enlarged significantly; in this case, the negative DC voltage intensity is large enough to produce secondary discharge, which will induce new vortices and jets to hinder the mainstream and eventually merge with the mainstream to form a new combined jet with a controllable direction.[14,15] This type of actuation has a higher ozone generation efficiency than DBD actuation and can generate a large area of surface discharge. The plasma extension length of sliding discharge can be stretched when the DC voltage amplitude is larger than a threshold value, until the whole distance between the AC and DC electrode is covered. For this reason, it is known as "tri-electrode sliding discharge" (TED).[16] The jet vector characteristics of the TED plasma actuator are studied experimentally and simulated. The results show that the intensity variation in the induced jet depends mainly on the frequency, polarity and amplitude of the applied negative DC voltage, and that the sliding discharge over a wide area can increase the body force and energy efficiency.[17,18]

Most of studies on EX-DBD and TED plasma actuation have focused on analyses of the discharge images and waveforms of the voltage and current. Measurements of the induced flow field have been obtained with low-speed PIV techniques. Although the use of the phase-locked method can improve the understanding of unsteady flow field characteristics, there are still some difficulties relating to the high-resolution spatiotemporal evolution of the plasma-induced flow field. In this paper, high-speed schlieren and high-speed particle image velocimetry (PIV) are used to analyze the high-resolution spatiotemporal structure of a flow field induced by plasma discharge, explore the effects of positive and negative DC voltages on the flow field induced by a typical DBD actuator, study the evolution trend in the induced flow, and further obtain a method that can improve the energy use and efficiency of plasma flow control.

2. Experimental procedure

The plasma actuator used in this experiment was comprised of three copper foil electrodes, each with a thickness of $T = 0.3$ mm (see Fig. 1), two exposed electrodes and one encapsulated electrode separated by a polytetrafluoroethylene dielectric plate with a thickness of $H = 1$ mm and a relative permittivity of $\varepsilon = 2.17$, which served as an insulating material. The two exposed electrodes were $W_1 = 5$-mm wide, and the encapsulated electrode was $W_2 = 40$-mm wide. The three electrodes each had a spanwise length of 80 mm and a thickness of 35 μm.

Listed in Table 1 are the cases that were to be tested in the present investigation, which can be classified as the DBD, tri-electrode sliding discharge (TED), and extended DBD (EX-DBD) mode. In Cases 1–3, a high AC voltage was applied across electrodes #1 and #2, and a high DC bias was applied to electrode #3 with different polarities. Electrode #1 was connected to a high-voltage sinusoidal AC wave source (model CTP-2000 K, CORONA Lab.), and the peak-to-peak voltage V_{AC} was set to be 16 kV. The carrier frequency was fixed at

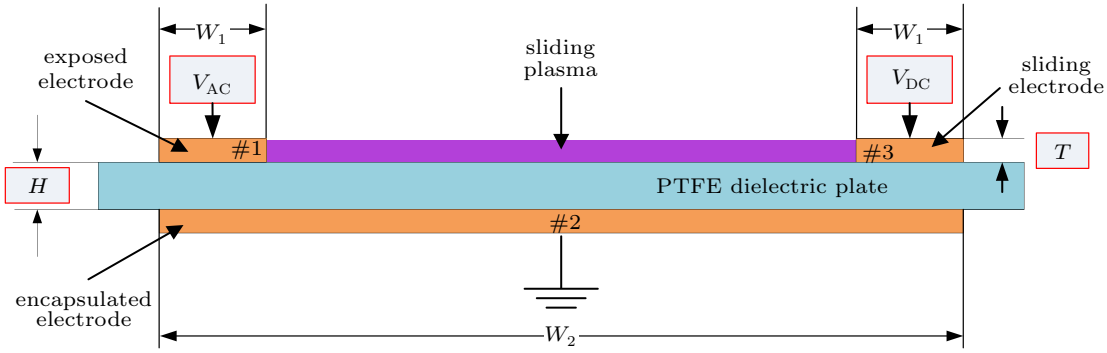


Fig. 1. Schematic illustration of tri-electrode plasma actuator.

$F = 8.25$ kHz, which is the optimal impedance frequency for this AC power supply. Encapsulated electrode #2 was grounded. Electrode #3, which can be called a "sliding electrode", was connected to a high-voltage DC power source with a voltage range from −18 kV to 18 kV to generate a sliding discharge (connected to a negative DC bias) or extended DBD actuation (connected to a positive DC bias).

Table 1. Experimental summary, V_{AC} and V_{DC} represent pulsed AC and DC high voltages, respectively; GND refers to grounding.

Case	Electrode #1	Electrode #2	Electrode #3	Abbreviation
1	AC	GND	GND	DBD
2	AC	GND	−DC	TED
3	AC	GND	+DC	EX-DBD

A high-speed phase-locked PIV system was adopted to quantitatively measure the instantaneous flow fields induced by plasma actuation. The camera was set to have a field of view (FOV) of approximately 105 mm × 63 mm. The frame rate was set to be at 1000 Hz per second with a resolution of 160 × 100 pixels and an exposure time of 200 μs. For each experimental case, five successive plasma pulses (with a burst frequency of $f_p = 5$ Hz) were recorded every 1 s. The final interrogation window size and overlap ratio used in the PIV cross-correlation procedure were 32 × 32 pixels and 75%, respectively. The PIV approach has previously been described in Ref. [16]. In both this paper and Ref. [16] the flow field induced by a tri-electrode plasma actuator was studied. The difference between these two papers is that the actuators are connected to AC and DC power supplies by different methods, the flow field structures are significantly different. In Ref. [16], electrode #1 was connected to a DC bias, electrode #2 was connected to an AC voltage source, and electrode #3 was grounded. A combined jet can be formed by the convergence of two oppositely directed starting vortices, and the direction of the combined jet can be driven by changing the polarity and amplitude of the DC voltage. In contrast, in this paper, electrode #1 was connected to an AC voltage source, and electrode #2 was grounded. When different DC biases are applied to electrode #3, the induced flow field develops freely from left to right, and the intensity of the induced flow field is changed greatly.

A high-speed schlieren system was used to qualitatively visualize the dynamic evolution of the vortex structures induced by these plasma actuators. A Phantom v2512 ultrahigh-speed camera was used for implementing image acquisition. The maximum spatial resolution and minimum exposure time of the camera were 1280 × 800 pixels and 1 μs, respectively. The maximum acquisition frequency was 25700 Hz, but an acquisition frequency of 10000 Hz was selected for this experiment. The system layout is similar to that in Ref. [17]. The difference between this paper and Ref. [17] is that the four-electrode plasma actuator studied in Ref. [17] can generate two starting vortices that move in opposite directions simultaneously, whereas the tri-electrode plasma actuator in this paper can produce only a main vortex such as the flow field of a typical DBD actuation.

3. Results

The data obtained through high-speed schlieren visualization and PIV measurements are analyzed to qualitatively and quantitatively characterize the dynamic evolution of the flow field structures induced by the plasma actuators (see Figs. 2–4). A burst frequency of $f_p = 5$ Hz (corresponding to a pulse period of $T_p = 1/f_p = 200$ ms) and a duty cycle of $\tau = 50\%$ were chosen for analyzing the unsteady flow structures. The PIV data set for the corresponding phase in each pulse period is summed and averaged via a self-programming process to obtain the phase-averaged results. No filtering method is used in any of the cases.

Figure 2 shows the formation and dynamic evolution of the starting vortices induced by a DBD at different times. When $t = 5$ ms ($t^* = 0.025$, and $t^* = t/T_p = t \times f_p$, where f_p is the burst frequency, T_p is the pulse period and t is time) or greater, due to the effect of convective diffusion, the pressure gradient acceleration allows the vorticity to enter into the ambient air from the plasma zone, and a starting vortex is generated at the juncture between electrode #1 and #2; the vortex then moves horizontally to the right. The starting vortices gradually expand and depart from the wall and then tend to become stable after approximately 20 ms ($t^* = 0.1$).

When high DC voltages with different polarities are applied to the sliding electrode, the induced flow will be considerably different.[16] This is because DBD actuation has different effects on the positive and negative half-cycles of AC voltage. Namely, the positive AC voltage half-cycle mainly produces plasma discharge, and the body force is primarily induced by the negative AC voltage half-cycle.[19,20] The negative DC component accelerates the drift of positive ions and triggers a larger number of more homogenous microdischarges in the positive half-cycle of the AC current, resulting in a stable and uniform plasma discharge zone, which causes the sliding discharge to cover the entire electrode gap. In contrast, the high positive DC voltage will increase the potential difference in the negative AC half-cycle, accelerate the negative charge carried by the negative long-lived O_2^- and O_3^- ions and generate a larger body force.[21] As the maximum induced velocity increases, the wall jet thickness generated by the electric field will increase, and the aerodynamic performance may be enhanced.

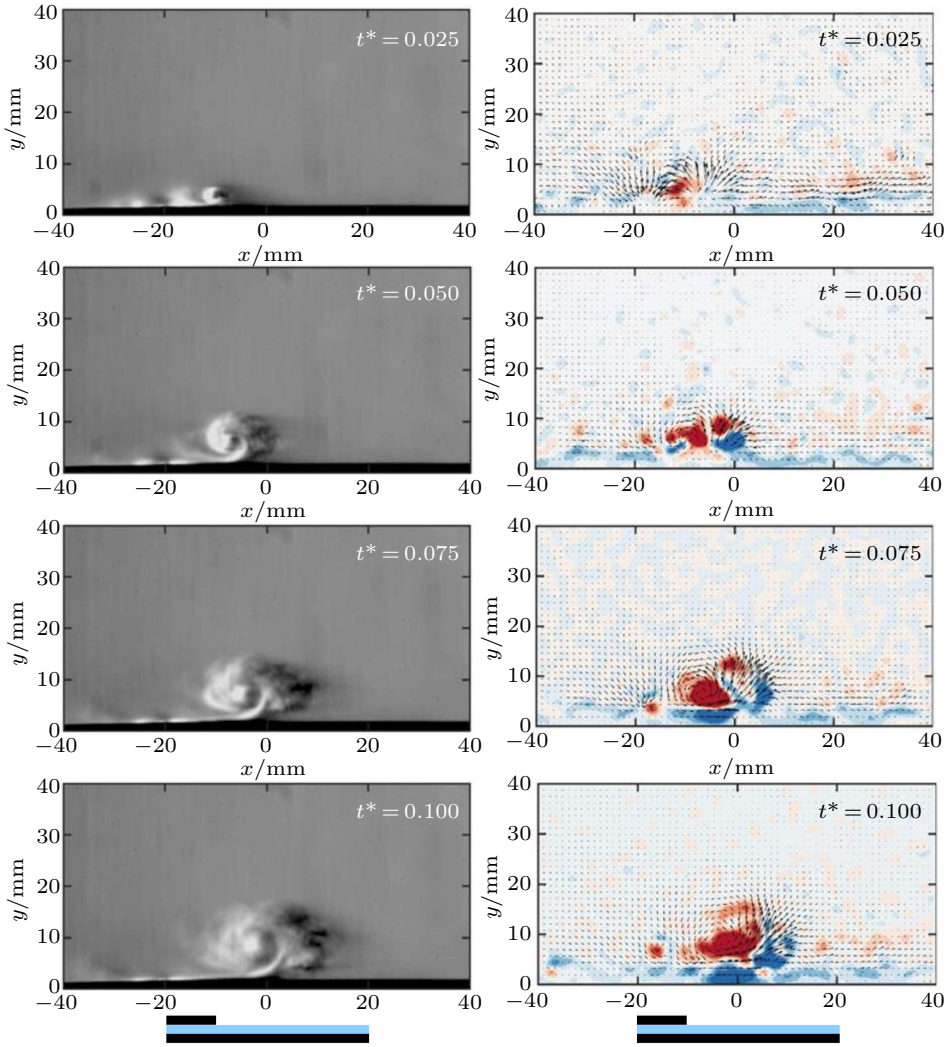


Fig. 2. Dynamic evolution of vortex structures induced by DBD actuation in Case 1, showing schlieren visualization results (left) and phase-averaged PIV results (right).

The induced flow field structures and functional areas of TED and DBD actuation are notably different. Due to the asymmetric positions of the exposed and encapsulated electrodes relative to the insulating layer, the DBD actuator will horizontally induce a vortex that develops freely from left to right (see Fig. 2); when the DBD actuator is affected by the negative DC bias, a tiny jet moving upward and to the left is generated near the sliding electrode ($t^* = 0.05$, $x = 19$ mm, $y = 0$ mm; see Fig. 3) and can impede the rightward horizontal free movement of the main vortex induced by the original DBD actuation. The collision between the main vortex and the tiny jet will enhance energy mixing in the near-wall region, causing the kinetic energy of the jet to accumulate in the area between the two exposed electrodes for a longer time than in the previous DBD case.

The PIV measurement results indicate that the vortex core induced by the DBD actuator moves from the position (-17.96 mm, 5.20 mm) at the 1st second (the current maximum vorticity $\omega_{\text{ext}} = 499.73\ \text{s}^{-1}$) to the position ($-1.43$ mm, 8.38 mm) at the 21st second and that the horizontal and vertical displacement speed of the vortex core are 0.83 m/s and 0.16 m/s, respectively. Moreover, the vortex core induced by the TED actuator moves from the position (-17.32 mm, 6.15 mm) at the 1st second to the position (-5.88 mm, 6.47 mm) at the 21st second, and the horizontal and vertical displacement speed of the vortex core are 0.57 m/s and 0.02 m/s, respectively, as shown in Table 2. The horizontal movement speed of the vortex induced by the TED actuator is greatly reduced due to the hindrance of the reverse tiny jet by the negative high DC voltage.

Combined with the schlieren results, the findings show that the vortex structure induced by DBD is horizontally stretched and that the vortex core moves at a higher speed in the horizontal direction than that in the TED case; this result is consistent with the conclusion in previous studies that the movement of the flow field induced by DBD is mainly in the horizontal direction and that the speed in the vertical direction is relatively low and can be neglected.[1,2] The vortex structure induced by TED remains substantially circular due to the flow collisions caused by the reverse jet induced by the high negative DC voltage and the formation of a "cavitation bubble" in a range of 0 mm–20 mm in the horizontal direction and 0 mm–10 mm in the vertical direction, which hinders a DBD-induced vortex from developing in the horizontal direc-

tion. In addition, the vortex structure associated with DBD actuation is more concentrated, undergoes less energy dissipation, and has a higher extreme value of vorticity than that in the TED case. Although the flow field induced by TED has a larger area of influence, within 20 ms after actuation begins, the field essentially covers the whole area between the two exposed electrodes (the horizontal distance from −20 mm to 20 mm), which suggests that the TED has a larger area influenced in the horizontal direction than the DBD.

As shown in Fig. 4 and Table 2, the EX-DBD yields an induced flow field structure similar to that the DBD does. The EX-DBD actuator causes the vortex core to move from (−17.96 mm, 5.20 mm) at the 1st second (the current maximum vorticity $\omega_{\text{ext}} = 477.88\ \text{s}^{-1}$) to (4.94 mm, 11.56 mm) at the 21st second (the current maximum vorticity $\omega_{\text{ext}} = 796.197\ \text{s}^{-1}$), and the horizontal and vertical displacement speed of the vortex core are 1.08 m/s and 0.25 m/s, respectively. Compared with those for the DBD and TED actuation, both the horizontal and vertical moving speed of maximum vorticity for the EX-DBD are greatly improved, but the growth rate of maximum vorticity is the slowest in the three types of actuations. Zheng *et al.* noted that[17] plasma discharge can cause charged ions to accumulate on the surface of the actuator under condition of no external airflow, which can result in the formation of a secondary electric field, and thus weakening the primary electric field and reducing the synthetic electric field on the surface of the actuator. This situation limits the flow control performance of the actuator. However, in a wind tunnel experiment, the charged ions on the surface of the actuator can be blown off by the incoming flow, the electromagnetic shielding effect will be greatly reduced, and the flow control performance might be enhanced.

Table 2. Analysis of positions of maximum vorticity. Vorticity and positions are in unit s^{-1} and in unit mm, respectively. $\Delta\omega$, Δx, and Δy are increments of vorticity and distance along x and y axes, respectively.

Case	Initial stage		Stable stage		Incremental analysis		
	$\omega_{\max}$	Position	$\omega_{\max}$	Position	$\Delta\omega$	Δx	Δy
DBD	499.73	−17.96, 5.20	1103.84	−1.43, 8.38	604.11	16.53	3.18
TED	308.37	−17.32, 6.15	672.07	−5.88, 6.47	363.70	11.44	0.32
EX-DBD	477.88	−16.69, 6.47	796.19	4.94, 11.56	318.31	21.63	5.09

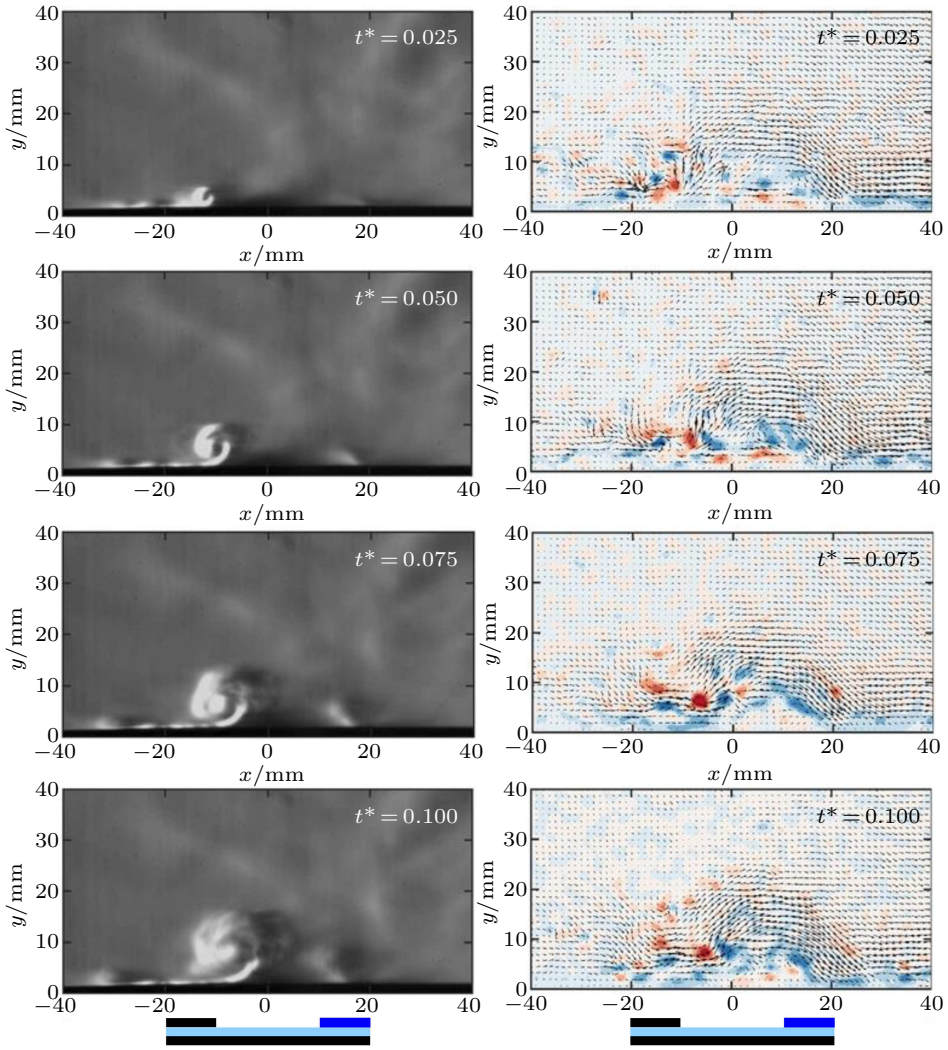


Fig. 3. Dynamic evolution of vortex structures induced by TED actuation in Case 2, showing schlieren visualization results (left) and phase-averaged PIV results (right).

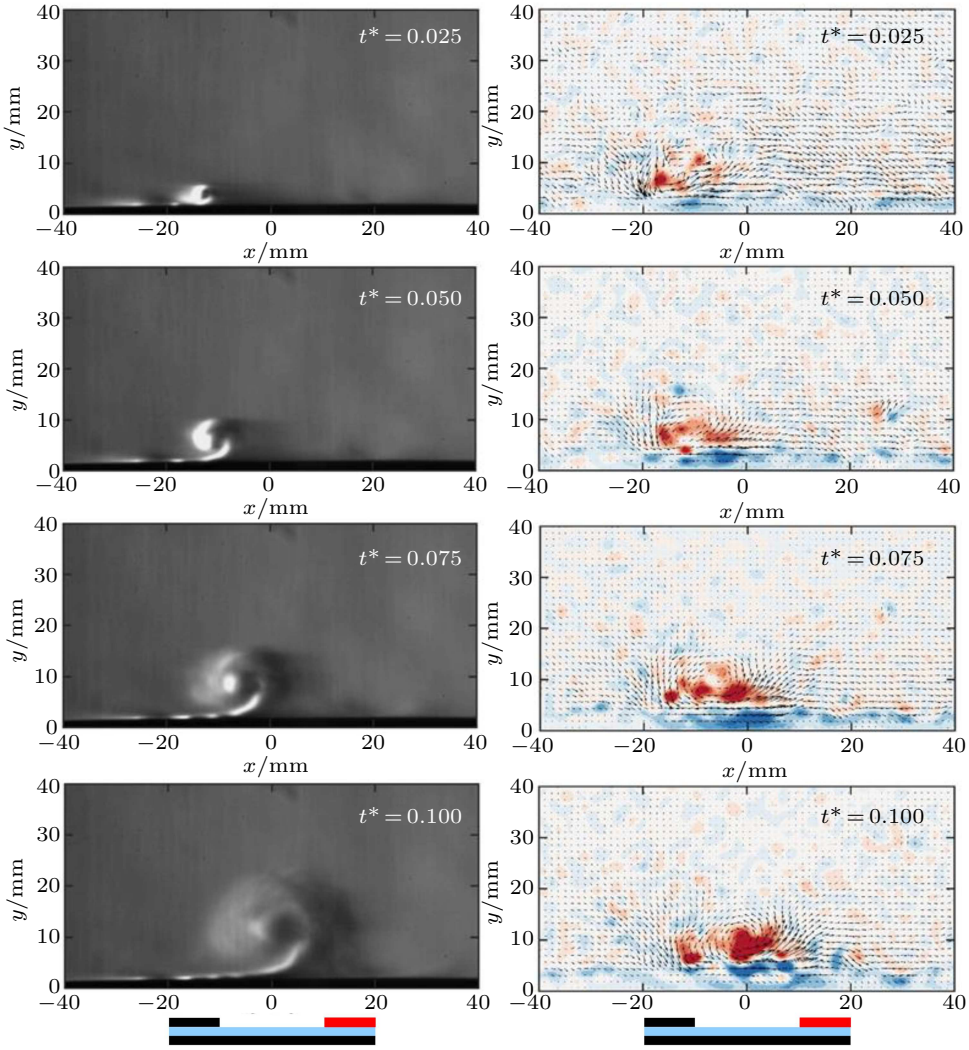


Fig. 4. Dynamic evolution of the vortex structures induced by EX-DBD actuation in Case 3, showing schlieren visualization results (left) and phase-averaged PIV results (right).

4. Analysis

In this section, we analyze the flow fields induced by the three types of actuations through comparing the dynamic evolution of the maximum horizontal velocity induced over time, the velocity profile at a fixed horizontal position, and the momentum and body forces in a fixed control volume.

4.1. Dynamic evolution of the maximum horizontal velocity over time

Figure 5 shows the comparison among the evolution processes of the maximum horizontal velocity induced by the three types of actuators over time, in which $t^* = 1$ corresponds to a pulsed frequency of 5 Hz with a duration of 200 ms. Basically, all three curves include an ascending stage, a stabilizing stage and a descending stage. The ascending stage of the maximum horizontal velocity curves of DBD and EX-DBD actuation are generally within the range of $t^* \leq 0.15$, and then they enter into the stabilizing and descending stages. When $0.15 \leq t^* \leq 0.25$, the induced velocities of DBD and EX-DBD actuation reach their own peak values and then rapidly decrease; subsequently, the curves enter into the first stage of velocity stabilization for a short period. Of the three types of actuations, the peak velocity of EX-DBD is the highest ($t^* = 0.15$, $U_{\max} = 2.81$ m/s), and the peak velocity of DBD is the lowest ($t^* = 0.13$, $U_{\max} = 1.73$ m/s). The duration ($\Delta t^* = 0.2$) of the velocity stabilization stage of DBD is greater than that of EX-DBD. When $t^* \geq 0.5$, the actuator is in the working gap of a pulsed discharge, and the maximum induced speed of DBD and EX-DBD decrease rapidly and then enter into the second speed stabilization stage. The duration of the second speed stabilization stage for DBD is greater than that for EX-DBD, accounting for approximately 40% of the entire cycle ($\Delta t^* = 0.4$). Overall, the energy attenuation of EX-DBD is faster than that of DBD.

The maximum induced velocity curve of TED is highly different from those of the other types of actuation: for example, there is only one speed stabilization stage, and the rate of velocity change is also relatively low. The ascending stage

of the TED curve lasts a longer time (up to $t^* = 0.3$) before reaching the peak velocity ($t^* = 0.39$, $U_{\max} = 2.41$ m/s), followed by the stabilizing stage ($0.3 \leq t^* \leq 0.5$); however, the descending stage has a shorter duration than those for the other two types of actuation. When $t^* \geq 0.5$, the maximum horizontal speed rapidly decreases and enters into a slow speed attenuation stage at $t^* = 0.7$.

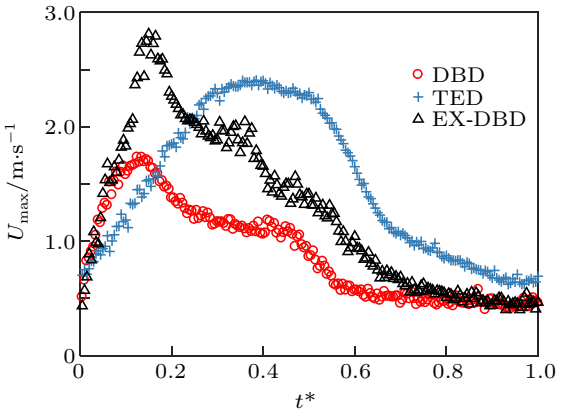


Fig. 5. Time evolution of maximum horizontal speed induced by different plasma actuators.

4.2. Analysis of velocity profiles

By selecting $t = 20$ ms ($t^* = 0.1$) and analyzing the horizontal velocity profiles of the jet for the 3 cases at $x = 0$ mm (the middle of the plasma actuator), the ability of the plasma actuators to induce jet flow and the efficiency of the conversion of pneumatic energy into electrical energy can be further studied. As shown in Fig. 6, the EX-DBD actuation yields a stronger induced jet intensity at the current time and position than the other actuations, and the maximum induced horizontal velocity peak ($U_{x,\text{EX-DBD}} = 1.94$ m/s) is higher than that of DBD ($U_{x,\text{DBD}} = 1.45$ m/s) and TED ($U_{x,\text{TED}} = 0.77$ m/s). However, the TED produces a peak velocity value at the position away from the wall surface ($y = 9.65$ mm), which is caused by the tiny backward jet induced by the high negative DC voltage; as a result, the jet interacts with the main flow, and a "cavitation bubble" forms in a range of 0 mm–10 mm

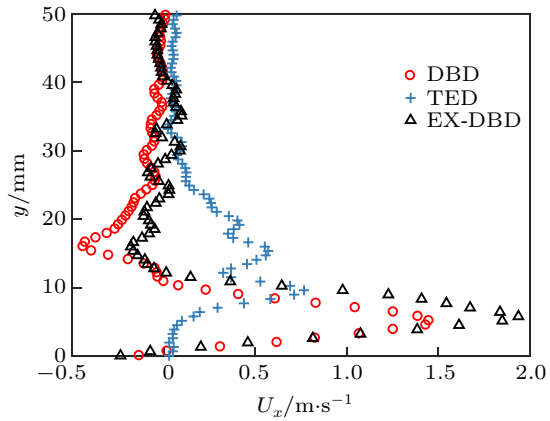


Fig. 6. Analysis of velocity profile of 3 cases for $x = 0$ mm and $t = 20$ ms.

in the vertical direction. Although the peak value of TED-induced horizontal velocity is the lowest in the three types of actuations, the corresponding profile thickness is much larger than those in the other two cases, which suggests that the TED has a larger area of influence in the vertical direction.

4.3. Analysis of momentum and body force

The body force induced by plasma actuation is extremely small [$O(1$ mN/m$^{-1})$] and difficult to measure directly and accurately. By analyzing the velocity field measured by PIV system, the momentum change and the body force change in the control volume can be calculated. This approach is currently commonly used in the efficiency evaluation of plasma actuators.[22] By analyzing the time-resolved PIV velocity fields, the horizontal component velocity of each PIV image is integrated to obtain the momentum $M_x = \rho \int_A U \mathrm{d}A$ and body force $F_x = \frac{\mathrm{d}M_x}{\mathrm{d}t}$ in the x direction for a fixed control volume, and the units of M_x and F_x are units N·s and N. The selected range of the control volume here is $x = -30 \sim 30$ mm and $y = 0 \sim 20$ mm. As shown in Fig. 7, the momentum peak of DBD and EX-DBD appear in the range of $t^* \leq 0.2$ and then slowly decay. The momentum peak of TED appears near $t^* = 0.4$, and this peak ($M_{x,\text{TED}} = 1.23 \times 10^{-3}$ N·s) is much higher than that for EX-DBD ($M_{x,\text{EX-DBD}} = 0.81 \times 10^{-3}$ N·s) and DBD ($M_{x,\text{DBD}} = 0.49 \times 10^{-3}$ N·s). The growth of momentum in the control volume is a result of plasma actuation and the energy dissipation caused by viscous resistance. When a pulsed AC voltage is applied to the plasma actuator, the flow effect induced by plasma actuation is stronger than the viscous resistance effect, and the starting vortex accelerates horizontally and propagates from left to right. In the pulsed discharge working gap, the plasma discharge becomes weaker, causing the vortex to be damped by air viscosity, and the momentum significantly decreases. Combined with compresensive analysis of Fig. 6 and Fig. 7, although the velocity peak and velocity profile height induced by TED are not so high as those induced by the other two types of actuation, the momentum peak value associated with the TED-induced jet is highest, and the duration of momentum growth is longest in the entire pulsed period. Thus, the duration of the body force generated by TED discharge lasts longer time than those in the other methods, and greater momentum can be injected into the ambient air. In addition, the TED actuation has a larger area of influence in the vertical direction and longer plasma extension in the horizontal direction than the other two types of actuations, which indicates that the TED actuation is more capable of creating a strong aerodynamic effect in a three-dimensional space above the surface of the actuator.

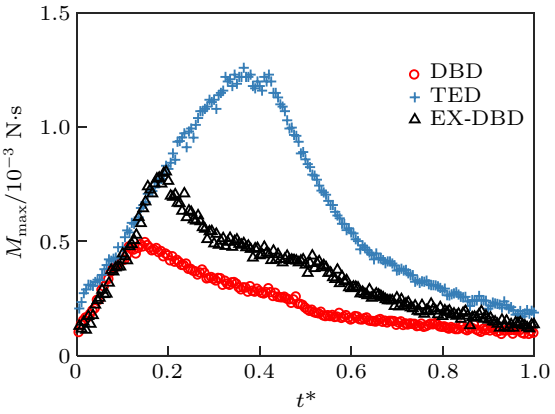


Fig. 7. Analysis of momentum in a control volume for 3 cases with $x = -30$ mm $\sim$ 30 mm and $y = 0$ mm $\sim$ 20 mm.

4.4. Analysis of the position of the vortex core

Figure 8 shows the evolution of the position of the vortex core over time for the three plasma actuators. When the plasma actuator is turned on, the induced vortex cores of the three plasma actuators move to the positive coordinates in the horizontal and vertical direction. The vortex core induced by EX-DBD actuation moves faster and further in the horizontal or vertical direction than the other two types of actuations. This is due to the fact that the high positive DC voltage will accelerate negative particles in the negative AC voltage half-cycle, resulting in stronger body force. As shown in Fig. 8(a),

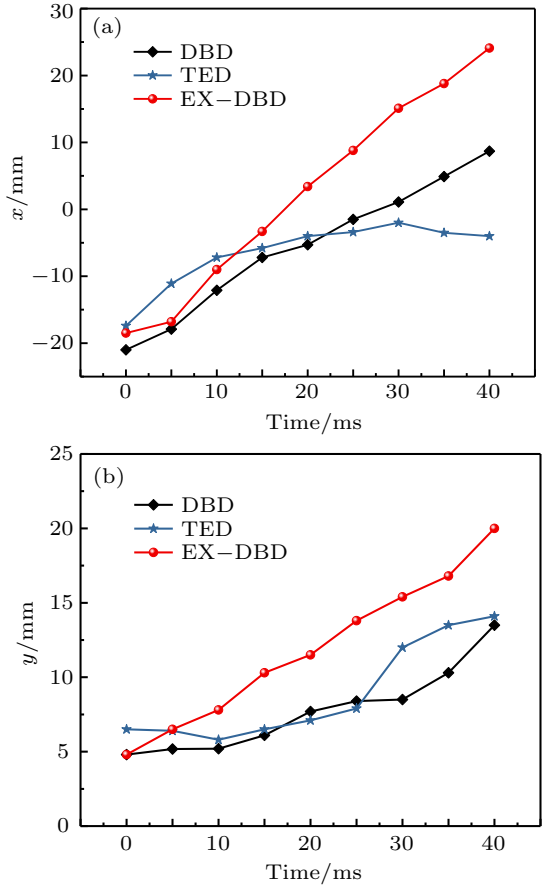


Fig. 8. (a) Horizontal position and (b) vertical position of vortex core varying with time for three plasma actuators.

the x-axis position of the vortex core of DBD continues to increase, indicating that the induced vortex moves at a constant speed from left to right in the horizontal direction. The x-axis position of the TED-induced vortex gradually increases at first, reaches a stable stage and then decreases gradually due to the reverse jet induced by the high negative DC voltage, which hinder the main flow from moving horizontally to the right. In Fig. 8(b), both TED and DBD grow slowly in the vertical direction, and the difference between their growth rates is small, indicating that their induced vortex cores move slowly in the vertical direction.

5. Conclusions

In this paper, high-speed PIV and high-speed schlieren system are used to analyze the dynamic evolution of the flow field induced by a three-electrode actuator. The experimental results show that the induced velocity peak value and profile velocity height of EX-DBD are higher than those of the other two types of actuations, suggesting that the temporal aerodynamic efficiency of EX-DBD is strongest. Due to the application of a high negative DC voltage at the sliding electrode, the TED actuation can not only enlarge the plasma zone extension but also induce a tiny backward jet to form near the sliding electrode. This jet collides with the mainstream and forms a "cavitation bubble" in a range of 0 mm–10 mm in the vertical direction. Although the intensity of the induced jet is not so strong as those for the other two types of actuations, The TED actuation has the longest duration in the entire pulsed period and the greatest influence on the height and width of the airflow near the wall surface. Thus, the TED is capable of generating strong aerodynamic effects in the three-dimensional space above the surface of the actuator. Although both the EX-DBD and the TED actuation display very good flow control performance, the experiments in this paper are performed in a static atmosphere. Plasma discharge can cause surface charge to accumulate, generate a secondary electric field, weaken the primary electric field, and reduce the potential difference in the plasma zone. Thus, the experimental conditions may have some influence on the plasma discharge and the flow control effect. In the future, wind tunnel experiments and computational fluid dynamics (CFD) simulations will be conducted to analyze the flow control effect and its associated mechanism in detail.

Acknowledgment

We would like to express our gratitude to Professor Zhengke Zhang of Northwestern Polytechnical University for his valuable technical guidance.

References

[1] Corke T C, Enloe C L and Wilkinson S P 2010 *Ann. Rev. Fluid Mech.* **42** 505

[2] Wang J J, Choi K S, Feng L H, Jukes T N and Whalley R D 2013 *Prog. Aerosp. Sci.* **62** 52

[3] Li Y H, Liang H, Wu Y, Wang J and Wei 2008 *J. Air Force Engineering University* **9** 5

[4] Wei B, Wu Y, Liang H, Zhu Y F, Chen J, Zhao G Y, Song H M and Jia M 2019 *Int. J. Heat Mass Transfer* **138** 163

[5] Zheng B R, Ge C, Ke X Z, Xue M and Wang Y S 2019 *AIAA* **2019** 0306

[6] Enloe C L, McLaughlin T E and VanDyken R D 2004 *AIAA J.* **42** 595

[7] Thomas F O, Corke T C, Iqbal M, Kozlov A and Schatzman D 2009 *AIAA J.* **47** 2169

[8] Zheng B R, Gao C, Li Y B, Feng L and Luo S J 2013 *Plasma Sci. Technol.* **15** 350

[9] Louste C, Artana G, Moreau E and Touchard G 2005 *J. Electrostat.* **63** 615

[10] Moreau E, Sosa R and Artana G 2008 *J. Phys. D: Appl. Phys.* **41** 115204

[11] Zheng B R, Chen J, Ge C, Ke X Z and Liang H 2019 *Proc. IMechE Part. G: J. Aerosp. Eng.* **233** 4788

[12] Moreau E, Louste C and Touchard G 2008 *J. Electrostat.* **66** 107

[13] Benard N and Moreau E 2014 *Exp. Fluids* **55** 1846

[14] Steven D S, Richard E H, William B, Liu D, Reeder M F and Stults J 2016 *AIAA J.* **54** 3313

[15] Steven D S, Richard E H, William B, Liu D, Reeder M F and Stults J 2011 *AIAA* **2011** 3732

[16] Zheng B R, Xue M, Ke X Z, Ge C, Wang Y S, Liu F and Luo S J 2019 *AIAA J.* **57** 467

[17] Zheng B R, Ke X Z, Ge C, Zhu Y F, Wu Y, Liu F and Luo S J 2020 *AIAA J.* **58** In Press

[18] Nishida H and Shiraishi T 2015 *AIAA J.* **53** 3483

[19] Soloviev V R and Krivtsov V M 2009 *J. Phys. D: Appl. Phys.* **42** 125208

[20] Gibalov V I and Pietsch G J 2000 *J. Phys. D: Appl. Phys.* **33** 2618

[21] Soloviev V R 2012 *J. Phys. D: Appl. Phys.* **45** 025205

[22] Whalley R D and Kwing S C 2012 *J. Fluid Mech.* **703** 192